Learning Mixtures of Smooth, Nonuniform Deformation Models for Probabilistic Image Matching

Nebojsa Jojic[1], **Patrice Simard**[1], **Brendan J. Frey**[2], **David Heckerman**[1]

[1]Microsoft Research
Redmond, Washington

[2]Computer Science
University of Waterloo

Abstract

By representing images and image prototypes by linear subspaces spanned by "tangent vectors" (derivatives of an image with respect to translation, rotation, *etc.*), impressive invariance to known types of uniform distortion can be built into feedforward discriminators. We describe a new probability model that can jointly cluster data and learn mixtures of nonuniform, smooth deformation fields. Our fields are based on low-frequency wavelets, so they use very few parameters to model a wide range of smooth deformations (unlike, *e.g.*, factor analysis, which uses a large number of parameters to model deformations). We give results on handwritten digit recognition and face recognition.

1 Introduction

Many computer vision and image processing tasks benefit from invariances to spatial deformations in the image. Examples include handwritten character recognition, face recognition and motion estimation in video sequences. When the input images are subjected to possibly large transformations from a *known* finite set of transformations (*e.g.*, translations in images), it is possible to model the transformations using a discrete latent variable and perform transformation-invariant clustering and dimensionality reduction using EM (Frey and Jojic 1999a; Jojic and Frey 2000). Although this method produces excellent results on practical problems, the amount of computation grows linearly with the total number of possible transformations in the input.

In many cases, we can assume the deformations are small, *e.g.*, due to dense temporal sampling of a video sequence, from blurring the input, or because of well-behaved handwriters. Suppose $(\boldsymbol{\delta}_x, \boldsymbol{\delta}_y)$ is a deformation field (a vector field that specifies where to shift pixel intensity), where $(\delta_{xi}, \delta_{yi})$ is the 2-D real vector associated with pixel i. Given a vector of pixel intensities $\mathbf{f}$ for an image, and assuming the deformation vectors are small, we can approximate the deformed image by

$$\tilde{\mathbf{f}} = \mathbf{f} + \frac{\partial \mathbf{f}}{\partial x} \circ \boldsymbol{\delta}_x + \frac{\partial \mathbf{f}}{\partial y} \circ \boldsymbol{\delta}_y, \tag{1}$$

where $\circ$ is element-wise product and $\partial \mathbf{f}/\partial x$ is a gradient image computed by shifting the original image to the right a small amount and then subtracting off the original image. Suppose $\boldsymbol{\delta}_y = \mathbf{0}$ and $\boldsymbol{\delta}_x = \alpha \mathbf{1}$, where α is a scalar. Then, (1) shifts the image to the right by an amount proportional to α. Fig. 1 shows some more complex examples of deformations computed in this way.

Simard *et al.* (1992, 1993) considered a deformation field that is a linear combination of the uniform fields for translation, rotation, scaling and shearing plus the nonuniform field for line thickness. When the deformation field is parameterized by a scalar α (*e.g.*, x-translation), $\frac{\partial \mathbf{f}}{\partial x} \circ \boldsymbol{\delta}_x + \frac{\partial \mathbf{f}}{\partial y} \circ \boldsymbol{\delta}_y$ can be viewed as the gradient of $\mathbf{f}$ with respect to α. Since the above approximation holds for small α, this gradient is tangent to the true 1-D deformation manifold of $\mathbf{f}$.

By processing the input from coarse to fine resolution, this tangent-based construction of a deformation field has also be used to model large deformations in an approximate manner (Vasconcelos and Lippman 1998).

The tangent approximation can also be included in generative models, including linear factor analyzer models (Hinton *et al.*, 1997) and nonlinear generative models (Jojic and Frey 2000).

Another approach to modeling small deformations is to jointly cluster the data and *learn* a locally linear deformation model for each cluster, *e.g.*, using EM in a factor analyzer (Ghahramani and Hinton 1997). An advantage of this approach over the tangent approach is that the types of deformation need not be specified beforehand. So, unknown, nonuniform types of defor-

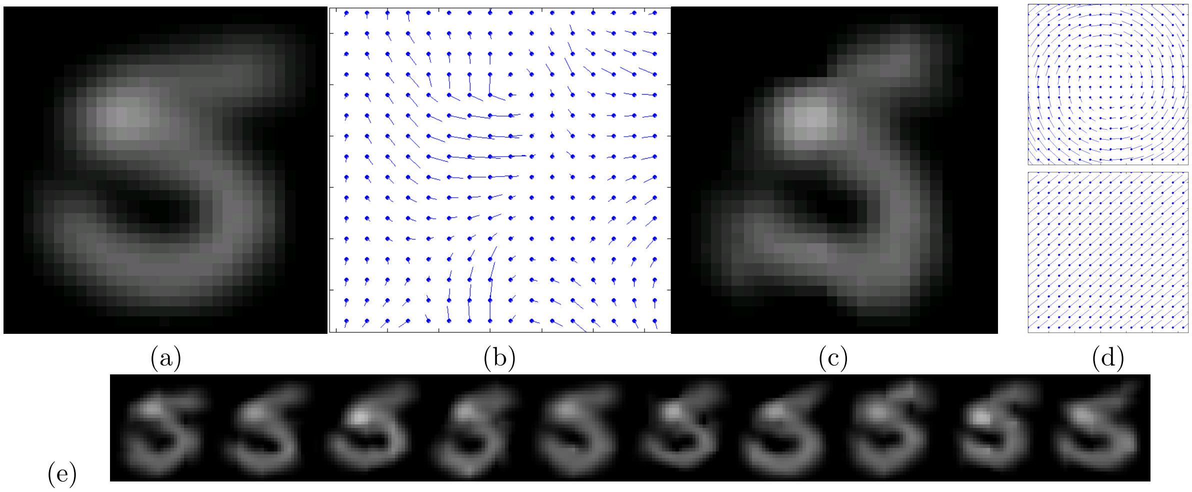

Figure 1: (a) An image of a hand-written digit. (b) A smooth, non-uniform deformation field. (c) The resulting deformed image. (d) Rotation and translation deformation fields. (e) Examples of deformed images produced by learned distributions over wavelet-based fields.

mation can be learned. However, a large amount of data is needed to accurately model the deformations, and learning is susceptible to local optima that confuse deformed data from one cluster with data from another cluster. (Some factors tend to "erase" parts of the image and "draw" new parts, instead of just perturbing the image.)

We describe a new probability model that can jointly cluster data and learn mixtures of nonuniform, smooth deformation fields. In contrast to the tangent approach, where the deformation field is a linear combination of prespecified uniform deformation fields (such as translation), in our model the deformation field is a linear combination of low-frequency wavelets. A mixture model of these wavelet coefficients is learned from the data, so our model can capture multiple types of nonuniform, smooth image deformations. In contrast to factor analysis, using a low-frequency wavelet basis allows our model to use significantly fewer parameters to represent a wide range of realistic deformations. For example, our model is much less likely to use a deformation field to "erase" part of an image and "draw" a new part, since the necessary field is usually not smooth.

In contrast with usual probabilistic deformation models, our generative model also incorporates the idea of "symmetric tangent distance" (Simard *et al*, 1993) by including deformations of the observed image. This leads to the idea of maximizing the likelihood of matching an observed image, instead of the likelihood of generating the observed image. However, under easily satisfiable conditions, the model reduces to the pure generative model. This symmetry allows the linear model for deformations to hold for larger transformations, as the prototype image and the observed image are both deformed to achieve a match.

Finally, our model is also related to the idea of separating style and content (Tenenbaum and Freeman, 1997), as the deformation linearization also leads to bilinear models that can be learned by exact EM.

2 Smooth, wavelet-based deformation fields

We ensure the deformation field $(\boldsymbol{\delta}_x, \boldsymbol{\delta}_y)$ is smooth by constructing it from low-frequency wavelets,

$$\boldsymbol{\delta}_x = \mathbf{R}\mathbf{a}_x, \qquad \boldsymbol{\delta}_y = \mathbf{R}\mathbf{a}_y, \tag{2}$$

where the columns of $\mathbf{R}$ contain low-frequency wavelet basis vectors, and $\mathbf{a} = \begin{bmatrix} \mathbf{a}_x \\ \mathbf{a}_y \end{bmatrix}$ are the deformation coefficients. We use a number of deformation coefficients that is a small fraction of the number of pixels in the image. (In contrast, each factor in factor analysis has a number of coefficients that is *equal* to the number of pixels.)

An advantage of wavelets is their space/frequency localization. The global trends in the image can be captured in the low-frequency coefficients while at the same time, the deformations localized in smaller regions of the image can be expressed by more spatially localized wavelets.

The deformed image can be expressed as

$$\tilde{\mathbf{f}} = \mathbf{f} + (\mathbf{G}_x\mathbf{f}) \circ (\mathbf{R}\mathbf{a}_x) + (\mathbf{G}_y\mathbf{f}) \circ (\mathbf{R}\mathbf{a}_y), \tag{3}$$

where the derivatives in (1) are approximated by sparse matrices $\mathbf{G}_x$ and $\mathbf{G}_y$ that operate on $\mathbf{f}$ to compute finite differences.

(3) is bilinear in the deformation coefficients $\mathbf{a}$ and the original image $\mathbf{f}$, *i.e.*, it is linear in $\mathbf{f}$ given $\mathbf{a}$ and it is linear in $\mathbf{a}$ given $\mathbf{f}$. To rewrite the element-wise product as a matrix product, we convert either the vector $\mathbf{Gf}$ or the vector $\mathbf{Ra}$ to a diagonal matrix using the diag() function:

$$\tilde{\mathbf{f}} = \mathbf{f} + \mathbf{D}(\mathbf{f})\mathbf{a}, \qquad (4)$$

$$\text{where } \mathbf{D}(\mathbf{f}) = [\text{diag}(\mathbf{G}_x\mathbf{f})\mathbf{R} \quad \text{diag}(\mathbf{G}_y\mathbf{f})\mathbf{R}]$$

$$\tilde{\mathbf{f}} = \mathbf{T}(\mathbf{a})\mathbf{f}, \qquad (5)$$

$$\text{where } \mathbf{T}(\mathbf{a}) = [\mathbf{I} + \text{diag}(\mathbf{R}\mathbf{a}_x)\mathbf{G}_x + \text{diag}(\mathbf{R}\mathbf{a}_y)\mathbf{G}_y]\,.$$

The first equation shows by applying a simple pseudo inverse, we can estimate the coefficients of the image deformation that transforms $\mathbf{f}$ into $\tilde{\mathbf{f}}$: $\mathbf{a} = \mathbf{D}(\mathbf{f})^{-1}(\tilde{\mathbf{f}} - \mathbf{f})$. This low-dimensional vector of coefficients minimizes the distance $||\mathbf{f} - \tilde{\mathbf{f}}||$. Under easily satisfied conditions on the differencing matrices $\mathbf{G}_x$ and $\mathbf{G}_y$, $\mathbf{T}(\mathbf{a})$ in (5) can be made invertible regardless of the image $\mathbf{f}$, so that $\mathbf{f} = \mathbf{T}(\mathbf{a})^{-1}\tilde{\mathbf{f}}$.

Given a test image $\mathbf{g}$, we could match $\mathbf{f}$ to $\mathbf{g}$ by computing the deformation coefficients, $\mathbf{a} = \mathbf{D}(\mathbf{f})^{-1}(\mathbf{g} - \mathbf{f})$, that minimize $||\mathbf{f} - \mathbf{g}||$. However, more extreme deformations can be successfully matched by deforming $\mathbf{g}$ as well:

$$\tilde{\mathbf{g}} = \mathbf{g} + (\mathbf{G}_x\mathbf{g}) \circ (\mathbf{R}\mathbf{b}_x) + (\mathbf{G}_y\mathbf{g}) \circ (\mathbf{R}\mathbf{b}_y), \qquad (6)$$

where $\mathbf{b}$ are the deformation coefficients for $\mathbf{g}$. The difference between the two deformed images is

$$\tilde{\mathbf{f}} - \tilde{\mathbf{g}} = \mathbf{f} - \mathbf{g} + [\mathbf{D}(\mathbf{f}) - \mathbf{D}(\mathbf{g})] \begin{bmatrix} \mathbf{a} \\ \mathbf{b} \end{bmatrix}. \qquad (7)$$

Again, minimizing $||\tilde{\mathbf{f}} - \tilde{\mathbf{g}}||$ is a simple quadratic optimization with respect to the deformation coefficients $\mathbf{a}$, $\mathbf{b}$. To favor some deformation fields over others, we can include a cost term that depends on the deformation coefficients.

Finally, a versatile image distance can be defined as:

$$d(\mathbf{f}, \mathbf{g}) = \min_{\mathbf{a},\mathbf{b}} \left\{ (\tilde{\mathbf{f}} - \tilde{\mathbf{g}})'\mathbf{\Psi}^{-1}(\tilde{\mathbf{f}} - \tilde{\mathbf{g}}) + [\mathbf{a}' \quad \mathbf{b}']\mathbf{\Gamma}^{-1} \begin{bmatrix} \mathbf{a} \\ \mathbf{b} \end{bmatrix} \right\} \qquad (8)$$

Matrix $\mathbf{\Psi}$ is a diagonal matrix whose non-zero elements contain variances of appropriate pixels. This distance allows different pixels to have different importance. For example, if we are matching two images of a tree in the wind, the deformation coefficients should be capable of aligning the trunk and large branches, while the variability in the appearance of the leaves would be captured in $\mathbf{\Psi}$. $\mathbf{\Gamma}$ captures the covariance structure of the wavelet coefficients of the allowed deformations. This distance can be used in the same applications as tangent distance, but being Bayesians (Patrice excluded!), we proceed with a probabilistic model.

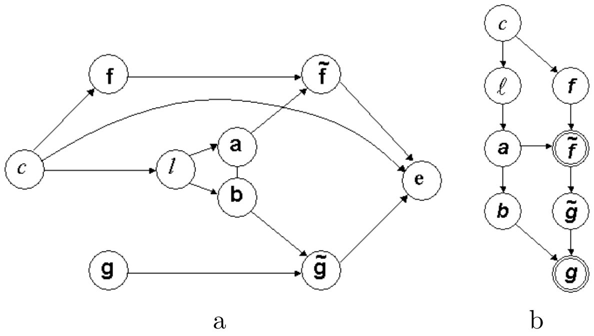

Figure 2: (a) A Bayes net for deformable image matching. (b) A generative version of the net conditioned on $\mathbf{e} = \mathbf{0}$.

3 Bayes net for deformable image matching

In Fig. 2a we show a Bayes net that can be used to compute the likelihood that the input image matches the images modeled by the network. For classification, we learn one of these networks for each class of data.

The generative matching process begins by clamping the test image $\mathbf{g}$. Then, an image cluster index c is drawn from $P(c)$ and given c, a latent image $\mathbf{f}$ is drawn from a Gaussian, $\mathcal{N}(\mathbf{f}; \boldsymbol{\mu}_c, \mathbf{\Phi}_c)$. In this paper, we assume $\mathbf{\Phi}_c = \mathbf{0}$, so $p(\mathbf{f}|c) = \delta(\mathbf{f} - \boldsymbol{\mu}_c)$. This allows us to use exact EM to learn the parameters of the model. We are investigating techniques which would allow us to learn $\mathbf{\Phi}_c$ as well.

Next, a deformation type index ℓ is picked according to $P(\ell|c)$. This index determines the covariance $\mathbf{\Gamma}_l$ of the deformation coefficients for both the latent image $\mathbf{f}$ and the test image $\mathbf{g}$:

$$p(\begin{bmatrix} \mathbf{a} \\ \mathbf{b} \end{bmatrix} |\ell) = \mathcal{N}(\begin{bmatrix} \mathbf{a} \\ \mathbf{b} \end{bmatrix}; \mathbf{0}, \mathbf{\Gamma}_\ell). \qquad (9)$$

$\mathbf{\Gamma}_\ell$ could be a diagonal matrix with larger elements corresponding to lower-frequency basis functions, to capture a wide range of smooth non-uniform deformations. However, $\mathbf{\Gamma}_\ell$ could also capture correlations among deformations in different parts of the image. The deformation coefficients for the latent image $\mathbf{a}$ and for the observed image $\mathbf{b}$ should be strongly correlated, so we model the joint distribution instead of modeling $\mathbf{a}$ and $\mathbf{b}$ separately.

Once the deformation coefficients $\mathbf{a}$, $\mathbf{b}$ have been generated, the deformed latent image $\tilde{\mathbf{f}}$ and the deformed test image $\tilde{\mathbf{g}}$ are produced from $\mathbf{f}$ and $\mathbf{g}$ according to (3) and (6). Using the functions $\mathbf{D}()$ and $\mathbf{T}()$ introduced above, we have

$$p(\tilde{\mathbf{f}}|\mathbf{f}, \mathbf{a}) = \delta(\tilde{\mathbf{f}} - \mathbf{f} - \mathbf{D}(\mathbf{f})\mathbf{a}) = \delta(\tilde{\mathbf{f}} - \mathbf{T}(\mathbf{a})\mathbf{f}), \qquad (10)$$

$$p(\tilde{\mathbf{g}}|\mathbf{g}, \mathbf{b}) = \delta(\tilde{\mathbf{g}} - \mathbf{g} - \mathbf{D}(\mathbf{g})\mathbf{b}) = \delta(\tilde{\mathbf{g}} - \mathbf{T}(\mathbf{b})\mathbf{g}). \qquad (11)$$

As an illustration of the generative process up to this point, in Fig. 1 we show several images produced by randomly selecting 8 deformation coefficients from a unit-covariance Gaussian and applying the resulting deformation field to an image.

The last random variable in the model is an error image $\mathbf{e}$ (called a "reference signal" in control theory), which is formed by adding a small amount of diagonal Gaussian noise to the difference between the deformed images $\tilde{\mathbf{f}}$ and $\tilde{\mathbf{g}}$:

$$p(\mathbf{e}|\tilde{\mathbf{f}}, \tilde{\mathbf{g}}, c) = \mathcal{N}(\mathbf{e}; \tilde{\mathbf{f}} - \tilde{\mathbf{g}}, \mathbf{\Psi}_c). \tag{12}$$

For good model parameters, it is likely that one of the cluster means can be slightly deformed to match a slightly deformed observed image. However, due to the constrained nature of these deformations, an exact match may not be achievable. Thus, to allow an exact match, the model helps the image difference with a small amount of non-uniform, cluster dependent noise. $\mathbf{\Psi}_c$ is diagonal and the non-zero elements contain the pixel variances. A natural place to include cluster dependence is in fact in the cluster noise $\mathbf{\Phi}_c$. Since we have chosen to collapse this noise model to zero, it is helpful to add cluster dependence into $\mathbf{\Psi}_c$.

This model can now be used to evaluate how likely it is to achieve a zero error image $\mathbf{e}$ by randomly selecting hidden variables conditioned on their parents in the fashion described above. If the model has the right cluster means, right noise levels and the right variability in the deformation coefficients, then the likelihood $p(\mathbf{e} = 0|\mathbf{g})$ will be high. Thus, this likelihood can be used for classification of images when the parameters of the models for different classes are known. Also, we can use the EM algorithm to estimate the parameters of the model that will maximize this likelihood for all observed images $\mathbf{g}_t$ in a training data set (see the Appendix).

By conditioning on $\mathbf{e} = \mathbf{0}$, we can transform the network into the generative network shown in Fig. 2b.[1]

After collapsing the deterministic nodes in the network, the joint distribution conditioned on the input $\mathbf{g}$ is

$$p(c, l, \mathbf{a}, \mathbf{b}, \mathbf{e}|\mathbf{g}) = P_{c,l}\mathcal{N}(\left[\begin{array}{c}\mathbf{a}\\ \mathbf{b}\end{array}\right]; 0, \mathbf{\Gamma}_\ell)\cdot$$
$$\cdot\,\mathcal{N}(\mathbf{e}; \boldsymbol{\mu}_c + \mathbf{D}(\boldsymbol{\mu}_c)\mathbf{a} - \mathbf{g} - \mathbf{D}(\mathbf{g})\mathbf{b}, \mathbf{\Psi}_c) \tag{13}$$

By integrating out the deformation coefficients we obtain $p(c, \ell, \mathbf{e}|\mathbf{g}) = P_{c,\ell}\mathcal{N}\left(\mathbf{e}; \boldsymbol{\mu}_c - \mathbf{g}, [\mathbf{\Psi}_c^{-1} - \mathbf{\Psi}_c^{-1}\mathbf{M}_c\mathbf{\Omega}_{c,\ell}\mathbf{M}'_c\mathbf{\Psi}_c^{-1}]^{-1}\right)$, where $\mathbf{M}_c = \left[\mathbf{D}(\boldsymbol{\mu}_c) \quad - \mathbf{D}(\mathbf{g})\right]$ and $\mathbf{\Omega}_{c,\ell} = (\mathbf{\Gamma}_\ell^{-1} + \mathbf{M}'_c\mathbf{\Psi}_c^{-1}\mathbf{M}_c)^{-1}$. This density function can be normalized over c, ℓ to obtain $P(c, \ell|\mathbf{e}, \mathbf{g})$. The likelihood can be computed by summing over the class and transformation indices:

$$p(\mathbf{e}|\mathbf{g}) = \tag{14}$$
$$\sum_{c,l} P_{c,l}\mathcal{N}\left(\mathbf{e}; \boldsymbol{\mu}_c - \mathbf{g}, [\mathbf{\Psi}_c^{-1} - \mathbf{\Psi}_c^{-1}\mathbf{M}_c\mathbf{\Omega}_{c,\ell}\mathbf{M}'_c\mathbf{\Psi}_c^{-1}]^{-1}\right)$$

By using this likelihood instead of the distance measure in (8), we are integrating over all possible deformations instead of finding the optimal deformation (which is given by (19) in the Appendix).

4 Experiments

We tested our algorithm on 20x28 greyscale images of people with different facial expressions and 8x8 greyscale images of handwritten digits from the CEDAR CDROM (Hull, 1994).

Deformable image matching. In Fig. 3a we estimate the optimal deformation fields necessary to match two images of a face of the same person but with different facial expression. We set the $\mathbf{\Psi}$ matrix to identity and we set $\mathbf{\Gamma}$ by hand to allow a couple of pixels of deformations. See Section 2 for nomenclature. In short, the two images $\mathbf{f}$ and $\mathbf{g}$ are shown left and right and the estimated flow fields that bring them together are shown next to each of them. In the middle are the deformed versions of the two images that together with the motion fields illustrate that the estimated deformations act to stretch the face on the right and make the face on the left smile, thus ending in similar images.

Comparison with the mixture of diagonal Gaussians (MDG). To compare our method with other generative models, we used a training set of 2000 images to learn 10 digit models using the EM algorithm and tested the algorithms on a test set of 1000 digit images. MDG needs 10-20 classes per digit to achieve the optimal error rate of only about 8% (Frey and Jojic 1999a) on the handwritten digit recognition task. Note that our network reduces to MDG when $\mathbf{\Gamma}_\ell$ is set to zero. To demonstrate the effectiveness of adding a deformation model to MDG, we trained our model with 15 classes per digit and only a single transformation model ($L = 1$) for all digits, with a total of 64 deformation coefficients (8 for each dimension in the latent and the observed images). In Fig. 3b we show one of the learned cluster means, the components in the corresponding deformation matrix $\mathbf{D}$ and the learned covariance matrix $\mathbf{\Gamma}$. $\mathbf{\Gamma}$ shows anticorrelation among the deformation coefficients for the latent and the observed image, as the network usually applies opposite deformations on these two images to achieve the match. However, there is also strong correlation between $\mathbf{b}_x$ and $\mathbf{b}_y$ and less correlation between $\mathbf{a}_x$

[1] To do so in a straightforward fashion, we assume that $|\mathbf{T}(\mathbf{b})| = 1$.

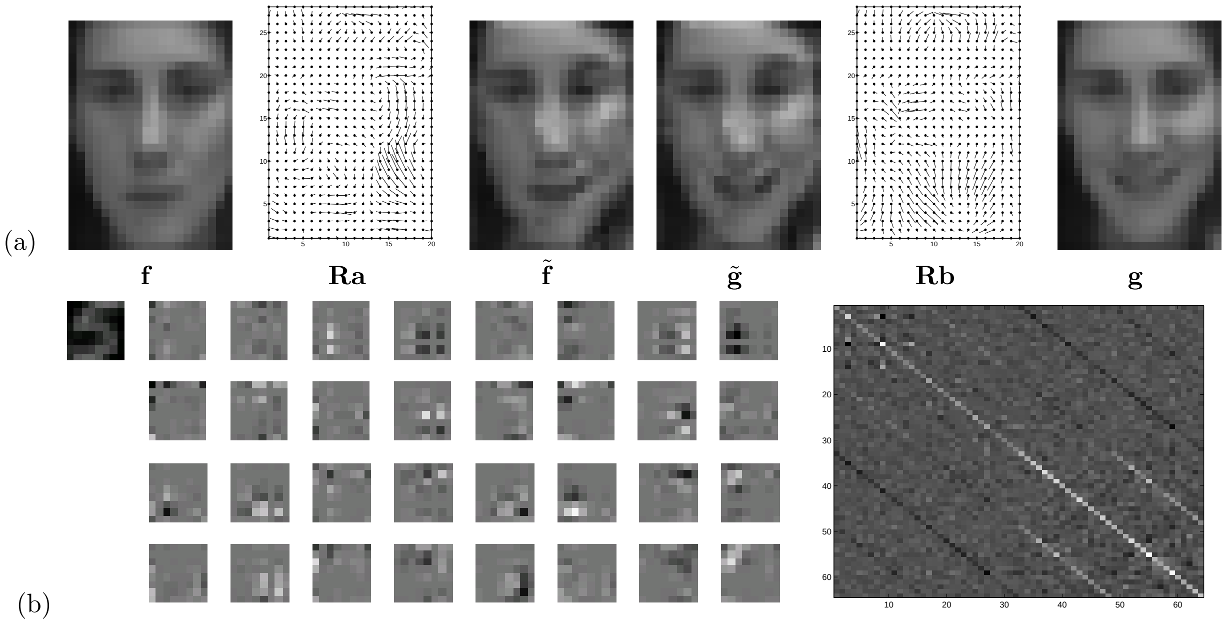

Mean $\boldsymbol{\mu}_c$ and components of $\mathbf{D}(\boldsymbol{\mu}_c)$ for one cluster

Matrix $\boldsymbol{\Gamma}$

Figure 3: Estimating the image deformation due to a change in facial expression and a subset of the learned parameters for the model of handwritten digits

and $\mathbf{a}_y$ as the network uses mostly a rotational adjustment on the input image, while the latent image is more freely deformed (Fig. 1e). Our model achieved the error rate of **3.6%**. Even if we keep only the diagonal elements in $\boldsymbol{\Gamma}$, the model achieves a 5% error rate.

Comparison with factor analysis. In factor analysis (FA) or in a mixture of factor analyzers (MFA), the deformation matrix $\mathbf{D}$ is called factor loading matrix and is not tied to the mean $\boldsymbol{\mu}_c$ as in our model (Fig. 3b). The factor covariance matrix is set to the identity matrix, as the extra freedom in the choice of the factor variances can be captured in the factor loading matrix. So, while FA/MFA try to capture the variability in the data by learning the components in the factor loading matrix and keeping the distribution over the factors fixed, our model does the opposite by tying the factor loading matrix to the mean image and learning the distribution over the factors (deformation coefficients). By doing this, we we are able to expand other images using the same deformation model. This allows us to share the deformation model across clusters and also to deform the input images. The comparable error rate in classification of handwritten digits for FA/MFA (3.3%) and our model (3.6%) indicates that most of the variability in images of handwriten digits can be captured by modeling smooth, non-uniform deformations without allowing full FA learning.

5 Conclusions

Our deformable image matching network could be used for a variety of computer vision tasks such as optical flow estimation, deformation invariant recognition and modeling correlations in deformations. For example, our learning algorithm could learn to jointly deform the mouth and eyes when modeling facial expressions.

References

A. P. Dempster, N. M. Laird and D. B. Rubin 1977. Maximum likelihood from incomplete data via the EM algorithm. *Proceedings of the Royal Statistical Society* B-39, 1–38.

B. J. Frey and N. Jojic 1999a. Estimating mixture models of images and inferring spatial transformations using the EM algorithm. *Proceedings of the IEEE Conference on Computer Vision and Pattern Recognition*, Ft. Collins, CO. IEEE Computer Society Press, Los Alamitos, CA.

Z. Ghahramani and G. E. Hinton 1997. The EM algorithm for mixtures of factor analyzers. University of Toronto Technical Report CRG-TR-96-1. Available at www.gatsby.ucl.ac.uk/∼zoubin.

G. E. Hinton, P. Dayan and M. Revow 1997. Modeling the manifolds of images of handwritten digits. *IEEE Trans. on Neural Networks* **8**, 65–74.

N. Jojic and B. J. Frey 2000. Topographic transformation as a discrete latent variable. In S.A. Solla, T. K. Leen, and K.-R. Müller (eds) *Advances in Neural Information Processing Systems 12*, MIT Press, Cambridge, MA.

P. Y. Simard, Y. Le Cun and J. Denker 1993. Efficient pattern recognition using a new transformation distance. In S. J. Hanson, J. D. Cowan and C. L. Giles, *Advances in Neural Information Processing Systems 5*, Morgan Kaufmann, San Mateo, CA.

N. Vasconcelos and A. Lippman 1998. Multiresolution tangent distance for affine invariant classification. In M. I. Jordan and M. I. Kearns and S. A. Solla (eds) *Advances in Neural Information Processing Systems 10*, MIT Press, Cambridge, MA.

J. B. Tenenbaum and W. T. Freeman 1997. Separating style from content. In Adv. in Neural Info. Proc. Systems, volume 9, MIT Press, 1997.

Appendix: EM for deformable image matching network

To fit the network to a set of training data, we assume that the error images for the training cases are zero and estimate the maximum likelihood parameters using EM (Dempster *et al.* 1977). In deriving the M-step, both forms of the deformation equations (4) and (5) are useful, depending on which parameters are being optimized. Using $\langle\rangle$ to denote an average over the training set, the update equations are:

$$\begin{aligned}
P_{c,\ell} =& \langle P(c,\ell|\mathbf{e}_t=\mathbf{0},\mathbf{g}_t)\rangle \qquad (15)\\
\hat{\boldsymbol{\mu}}_c =& \langle\sum_\ell P(c,\ell|\mathbf{e}_t=\mathbf{0},\mathbf{g}_t)\mathrm{E}[\mathbf{T}(\mathbf{a})'\boldsymbol{\Psi}_c^{-1}\mathbf{T}(\mathbf{a})|c,\ell,\mathbf{e}_t=\mathbf{0},\mathbf{g}_t]\rangle^{-1}\\
&\cdot\langle\sum_\ell P(c,\ell|\mathbf{e}_t=\mathbf{0},\mathbf{g}_t)\mathrm{E}[\mathbf{T}(\mathbf{a})'\boldsymbol{\Psi}_c^{-1}\mathbf{T}(\mathbf{b})\mathbf{g}_t|c,\ell,\mathbf{e}_t=\mathbf{0},\mathbf{g}_t]\rangle, \qquad (16)\\
\hat{\boldsymbol{\Gamma}}_\ell =& \frac{\left\langle\sum_c P(c,\ell|\mathbf{e}_t=\mathbf{0},\mathbf{g}_t)\mathrm{E}\left\{\left[\begin{array}{c}\mathbf{a}\\ \mathbf{b}\end{array}\right][\mathbf{a}' \quad \mathbf{b}']\middle|c,\ell,\mathbf{e}_t=\mathbf{0},\mathbf{g}_t\right\}\right\rangle}{\langle\sum_c P(c,\ell|\mathbf{e}_t=\mathbf{0},\mathbf{g}_t)\rangle} \qquad (17)\\
\hat{\boldsymbol{\Psi}}_c =& \mathrm{diag}\left(\frac{\langle\sum_\ell P(c,l|\mathbf{e}_t=\mathbf{0},\mathbf{g}_t)\mathrm{E}[(\tilde{\mathbf{f}}-\tilde{\mathbf{g}}_t)\circ(\tilde{\mathbf{f}}-\tilde{\mathbf{g}}_t)|c,l,\mathbf{e}_t=\mathbf{0},\mathbf{g}_t]\rangle}{\langle\sum_\ell P(c,l|\mathbf{e}_t=\mathbf{0},\mathbf{g}_t)\rangle}\right) \qquad (18)
\end{aligned}$$

The expectations needed to evaluate the above update equations are given by:

$$\begin{aligned}
\boldsymbol{\Omega}_{c,\ell} = \mathrm{cov}\left\{\left[\begin{array}{c}\mathbf{a}\\ \mathbf{b}\end{array}\right]\middle|c,\ell,\mathbf{e}_t=\mathbf{0},\mathbf{g}_t\right\} =& (\boldsymbol{\Gamma}_\ell^{-1}+\mathbf{M}_c'\boldsymbol{\Psi}_c^{-1}\mathbf{M}_c)^{-1}\\
\boldsymbol{\gamma}_{c,\ell} = \mathrm{E}\left\{\left[\begin{array}{c}\mathbf{a}\\ \mathbf{b}\end{array}\right]\middle|c,l,\mathbf{e}_t=\mathbf{0},\mathbf{g}_t\right\} =& \boldsymbol{\Omega}_{c,\ell}^{-1}\mathbf{M}_c'\boldsymbol{\Psi}_c^{-1}(\boldsymbol{\mu}_c-\mathbf{g}_t) \qquad (19)\\
\mathrm{E}\left\{\left[\begin{array}{c}\mathbf{a}\\ \mathbf{b}\end{array}\right][\mathbf{a}' \quad \mathbf{b}']\middle|c,\ell,\mathbf{e}_t=\mathbf{0},\mathbf{g}_t\right\} =& \boldsymbol{\Omega}_{c,\ell}+\boldsymbol{\gamma}_{c,\ell}\boldsymbol{\gamma}_{c,\ell}' \qquad (20)\\
\mathrm{E}[(\tilde{\mathbf{f}}-\tilde{\mathbf{g}}_t)\circ(\tilde{\mathbf{f}}-\tilde{\mathbf{g}}_t)|c,l,\mathbf{e}_t=\mathbf{0},\mathbf{g}_t] = \big(\boldsymbol{\mu}_c-\mathbf{g}_t+\mathbf{M}_c\boldsymbol{\gamma}_{c,\ell}\big)&\circ\big(\boldsymbol{\mu}_c-\mathbf{g}_t+\mathbf{M}_c\boldsymbol{\gamma}_{c,\ell}\big)+\mathrm{diag}(\mathbf{M}_c(\boldsymbol{\Omega}_{c,\ell})\mathbf{M}_c')
\end{aligned}$$

Expectations in (16) are computed using

$$\begin{aligned}
\mathbf{T}(\mathbf{a})'\boldsymbol{\Psi}_c^{-1}\mathbf{T}(\mathbf{a}) = \boldsymbol{\Psi}_c^{-1} &+ \sum_{d\in\{x,y\}}\mathbf{G}_d'\mathrm{diag}(\mathbf{R}\mathbf{a}_d)\boldsymbol{\Psi}_c^{-1} \qquad (21)\\
&+\sum_{d\in\{x,y\}}\boldsymbol{\Psi}_c^{-1}\mathrm{diag}(\mathbf{R}\mathbf{a}_d)\mathbf{G}_d+\sum_{d_1,d_2\in\{x,y\}}\mathbf{G}_{d_1}'\boldsymbol{\Psi}_c^{-1}\mathrm{diag}(\mathbf{R}\mathbf{a}_{d_1}\mathbf{a}_{d_2}'\mathbf{R}')\mathbf{G}_{d_2}
\end{aligned}$$

$$\begin{aligned}
\mathbf{T}(\mathbf{a})'\boldsymbol{\Psi}_c^{-1}\mathbf{T}(\mathbf{b})\mathbf{g}_t = \boldsymbol{\Psi}_c^{-1}\mathbf{g}_t &+ \sum_{d\in\{x,y\}}\mathbf{G}_d'\mathrm{diag}(\mathbf{R}\mathbf{a}_d)\boldsymbol{\Psi}_c^{-1}\mathbf{g}_t \qquad (22)\\
&+\sum_{d\in\{x,y\}}\boldsymbol{\Psi}_c^{-1}\mathrm{diag}(\mathbf{R}\mathbf{b}_d)\mathbf{G}_d\mathbf{g}_t+\sum_{d_1,d_2\in\{x,y\}}\mathbf{G}_{d_1}'\boldsymbol{\Psi}_c^{-1}\mathrm{diag}(\mathbf{R}\mathbf{a}_{d_1}\mathbf{b}_{d_2}'\mathbf{R}')\mathbf{G}_{d_2}\mathbf{g}_t.
\end{aligned}$$

Then, the expectations $\mathrm{E}[\mathbf{a}]$ and $\mathrm{E}[\mathbf{b}]$ are the two halves of the vector $\boldsymbol{\gamma}_{c,\ell}$, while $\mathrm{E}[\mathbf{a}_{d_1}\mathbf{a}_{d_2}']$ and $\mathrm{E}[\mathbf{a}_{d_1}\mathbf{b}_{d_2}']$, for $d_1,d_2\in\{x,y\}$, are square blocks of the matrix in (20).